X-525-70-231

PREPRINT

NASA TM X-63984

RADIATION PATTERN CALCULATIONS FOR AN ATS-F 48-PANEL DEPLOYABLE-REFLECTOR ANTENNA

R. MIEZIS
R. F. SCHMIDT

JUNE 1970

GSFC — GODDARD SPACE FLIGHT CENTER —
GREENBELT, MARYLAND

X-525-70-231

RADIATION PATTERN CALCULATIONS FOR AN ATS-F 48-PANEL DEPLOYABLE-REFLECTOR ANTENNA

R. Miezis
Computer Applications, Inc.

R. F. Schmidt
Advanced Development Division
Goddard Space Flight Center

June 1970

Goddard Space Flight Center
Greenbelt, Maryland

CONTENTS

ILLUSTRATIONS

TABLES

RADIATION PATTERN CALCULATIONS FOR AN ATS-F 48-PANEL DEPLOYABLE-REFLECTOR ANTENNA

R. Miezis
Computer Applications, Inc.

R. F. Schmidt
Advanced Development Division
Goddard Space Flight Center

ABSTRACT

Far-field radiation patterns are computed for a deployable-reflector antenna composed of N' panels which are, ideally, sections of parabolic cylinder. The vector Kirchhoff diffraction method (physical-optics) is applied at the antenna surface, and integration is accomplished by digital computer to obtain the backscattered radiation patterns. Surface normals are found for indexed parabolic cylinders and distorted versions of this design structure approximating a paraboloid of revolution. It is shown that one of the methods evolved for a thermally distorted reflector is adaptable to the case when the assumption of straight lines on the metallized reflector mesh between supporting ribs is not justified.

GLOSSARY OF NOTATION

Symbol	Meaning
$\bar{E}$, $\bar{H}$	electric and magnetic field vectors, subscripted
$\bar{n}$	unit normal to a surface
ψ	scalar wave without time dependence, solution to wave equation
r	radial distance
E_r, E_θ, E_ϕ	spherical components of an electric-field
$\mathfrak{F}$	electric-field of directive source, or a generic symbol for a function
σ, ζ	radial and angular variables of a cylindrical coordinate net
F	focal length of a paraboloid
$\bar{\rho}$	position vector to surface
$\bar{\rho}_\sigma$, $\bar{\rho}_\zeta$	partial derivatives of $\bar{\rho}$ with respect to subscripted variable
F_c	focal length of a parabolic cylinder
F_R	focal length of a parabolic rib lying in a parabolic cylinder
a	antenna panel half-angle
$\bar{\tau}$	tangent to an arc or surface
$\bar{L}$	vector representing fabric line
$P_i(y)$	polynomial in variable y for i^{th} antenna rib
A, A^{-1}	classical rotation matrix and its inverse
$\hat{i}$, $\hat{j}$, $\hat{k}$	Cartesian base vectors
u, v	parameters for orthogonal net on parabolic cylinder
E, F, G	functions of u and v

GLOSSARY OF NOTATION (continued)

Symbol	Meaning
$\cap$	symbol for intersection
Θ, Φ	spherical angles for feed and surface discussion
θ, ϕ	spherical angles for observer
μ_0	permittivity of free space
ϵ_0	permeability of free space
z_0	intrinsic impedance of free space
x, y, z	Cartesian components of a vector
x_u, y_u, z_u	partial derivatives of x (u, v) with respect to u, etc.
x_v, y_v, z_v	partial derivatives of x (u, v) with respect to v, etc.
ds	differential area
LI	sampling interval in numerical integration
D, R_c	diameter and minimum radius of curvature of scattering object
λ	wavelength
$\bar{\rho}_\epsilon$	feed position vector
S	source strength of a feed element

RADIATION PATTERN CALCULATIONS FOR AN ATS-F 48-PANEL DEPLOYABLE-REFLECTOR ANTENNA

INTRODUCTION

Consideration of continuous reflecting surfaces with discontinuous derivatives for the Applications Technology Satellite (ATS-F) has led to the development of methods for computing normals, areas, etc. of such surfaces as required by the complex-vector Kirchhoff diffraction theory. Departure from the class of surfaces obtained by rotating arcs, derived by conic sections, has resulted in methods which are partially analytic and partially numeric in nature. For example, the normals to a parabolic-cylinder section can be obtained analytically, but the normals for 48 indexed sections of this type are injected into the program using the analysis for a single panel in conjunction with a 3×3 rigid-body rotation matrix. Actually, the mixture of analytical and numerical techniques is also seen with surfaces obtained through conic section, although to a lesser degree. In any event, the reader will not find a single equation, or even a set of equations, which can be combined to form a "master equation" for these diffraction problems. Rather, a process is developed, whereby the quantities required by the Kirchhoff formulation are made available to the computer for numerical integration.

A brief review of the mechanics of the Kirchhoff method is given here; the referenced documentation provides greater detail. In the far-field (Fraunhofer region) the general formulation for the electric field reduces to a single integral which contains a mathematical simulation of a sheet current that flows tangentially along a reflector surface.

$$\bar{E}(x', y', z') = -\frac{j \omega \mu}{4 \pi} \int_{s_1} \bar{n} \times \bar{H}_1 \psi \, d s$$

It can be seen that "gain" is implicit in the parameter ω (angular frequency). Also, it is noted that the vector cross product of the unit surface normal $\bar{n}$ with the magnetic field $\bar{H}_1$ necessarily results in a sheet current flowing along the local tangent to the surface. This is consistent with the physics of the situation and agrees with the intuitive concept of a current on a reflector antenna. Under the integral sign, the factor $\psi = e^{-ikr}/r$ is recognized as the product of a phase term, the periodicity of Young, and a space attentuation or divergence term.

Annexing differential area, ds, completes the simulation. The result is an integral over a collection of Huygens sources, in vector notation, for three-dimensional bodies that are perfectly conducting.

The preceding views the Kirchhoff formulation from the location of the observer of a field distribution. The calculation of the magnetic field distribution $\bar{H}_i$ at the reflector is an important preliminary detail which can be somewhat involved, depending on the feed complexity. Feed directivity, polarization, space divergence and periodicity between feed and reflector, and reflector boundary conditions are taken into account to obtain the distribution from the incident magnetic field $\bar{H}_i$. The relationship between the incident field and the distribution $\bar{H}_i$ which is integrated is

$$\bar{n} \times \bar{H}_i = 2\, \bar{n} \times \bar{H}_i$$

The boundary condition, therefore, enhances tangential $\bar{H}_i$ and annihilates normal $\bar{H}_i$. It is sufficient to calculate only the scattered field $\bar{E}(x', y', z')$ in the Fraunhofer region since $\bar{H}(x', y', z')$ differs from the former by only a physical constant $z_0 = \mu_0 / \epsilon_0$ and an orthogonal rotation in space. These scattered electric and magnetic fields are synchronous in time (cophased).

In summary, the vector Kirchhoff formulation deals with surfaces, and integration is over the actual antenna surface rather than over an "aperture-plane." The simulation closely adheres to the actual physical process involved in the illumination of the antenna by converting incident fields to electric sheet currents. Polarization, amplitude, and phase are carried throughout the entire problem, which is distinct from ray-optics analysis. Finally, since the present simulation deals with complex vectors, the results can be regarded as three spatially orthogonal complex-scalar solutions for each problem, of which only the transverse fields E_θ and E_ϕ are retained for the far-field, together with their respective phases.

ANALYTICAL APPROACH TO SURFACE NORMALS

The unit normals to a given surface can often be obtained in several ways, however, as the description of the surface becomes more tenuous some of these methods cease to be applicable. Prior to dealing with highly arbitrary surfaces, it is helpful to review a few standard approaches for well-known geometries. The subsequent transition to more general cases then becomes obvious. In the following discussion, no attempt is made to obtain an analytic "best-fit" surface

in the RMS sense, or any related approach, in order to obtain the normals. Instead, the goal is simply to provide the computer with the Cartesian components (n_x, n_y, n_z) of a unit normal for each curvilinear quadrilateral (differential area) where the surface may be specified by only a limited amount of data and perhaps some auxiliary constraint or assumption such as straight fabric lines.

The paneled antenna considered for ATS-F is a close approximation of a paraboloid. The latter is described by

$$x = \sigma \sin \zeta, \quad y = -\sigma \cos \zeta, \quad z = \frac{\sigma^2}{4F} + z_1, \quad (z_1 = \text{constant}),$$

and this parametric form will serve to introduce methods of computing normals. Another way of describing the same paraboloidal surface is

$$z = \mathfrak{F}_1(x, y) = \frac{x^2 + y^2}{4F} + z_1 \quad \text{or} \quad \mathfrak{F}_2(x, y, z) = \mathfrak{F}_1(x, y) - z = 0.$$

In one text[1], the unit normals to a surface are found using

$$\bar{n} = \left(-\frac{\partial z}{\partial x}\hat{i} - \frac{\partial z}{\partial y}\hat{j} + \hat{k} \right) \Big/ \left[\left(\frac{\partial z}{\partial x}\right)^2 + \left(\frac{\partial z}{\partial y}\right)^2 + 1 \right]^{1/2}$$

This method is a variation of the so-called gradient method.[2] The gradient method, in general terms, leads to the form

$$\bar{n} = -\frac{\nabla \mathfrak{F}_2(x, y, z)}{|\nabla \mathfrak{F}_2(x, y, z)|} = \left(-\hat{i}\frac{\partial \mathfrak{F}_2}{\partial x} - \hat{j}\frac{\partial \mathfrak{F}_2}{\partial y} - \hat{k}\frac{\partial \mathfrak{F}_2}{\partial z} \right) \Big/ \left[\left(\frac{\partial \mathfrak{F}_2}{\partial x}\right)^2 + \left(\frac{\partial \mathfrak{F}_2}{\partial y}\right)^2 + \left(\frac{\partial \mathfrak{F}_2}{\partial z}\right)^2 \right]^{1/2}.$$

$$= \left(-\hat{i}\frac{\partial \mathfrak{F}_1}{\partial x} - \hat{j}\frac{\partial \mathfrak{F}_1}{\partial y} + \hat{k} \right) \Big/ \left[\left(\frac{\partial \mathfrak{F}_1}{\partial x}\right)^2 + \left(\frac{\partial \mathfrak{F}_1}{\partial y}\right)^2 + 1 \right]^{1/2}$$

[1] Ref. 1, page 208
[2] Ref. 2, page 27 and Ref. 1, page 103

Another method of obtaining unit normals to surfaces is suggested by consideration of a pair of tangent lines at a point.[1] A normalized vector cross-product of the tangents is

$$\bar{n} = \bar{\rho}_\sigma \times \bar{\rho}_\zeta / |\bar{\rho}_\sigma \times \bar{\rho}_\zeta|$$

where $\bar{\rho} = \hat{i}\, x + \hat{j}\, y + \hat{k} z$ is the vector from the origin to the surface, and the subscripted $\bar{\rho}$ denotes partials with respect to the indicated parameter. The reader can verify that all three methods lead to the same result for the family of paraboloids given above:

$$\bar{n} = (-\hat{i}\sigma \sin\zeta + \hat{j}\,\sigma\cos\zeta + \hat{k}\,2F)/(\sigma^2 + 4F^2)^{1/2}$$

It is noted that all of the preceding methods are general in the sense that they can be applied to other parametric representations[2] for surfaces. A departure from surfaces of revolution will now be made, with the final objective of extending the technique to distorted surfaces and continuous surfaces with discontinuous derivatives.

The idealized paneled structure, approximately a true paraboloid on ATS-F, consists of indexed sections of a parabolic cylinder whose focal-length is taken as F_c (a line-focus). The normals to a parabolic cylinder described by

$$x = \sigma, \quad y = \text{any value}, \quad z = \frac{\sigma^2}{4F_c} + z_1, \quad (z_1 = \text{constant})$$

can be found using a variation of the gradient method since

$$z = \Im_1(x) = \frac{x^2}{4F_c} + z_1$$

[1] Ref. 1, page 209
[2] Ref. 3, page 13

now represents the surface. Then

$$\bar{n} = (-\sigma \hat{i} + 2 F_c \hat{k})/(\sigma^2 + 4 F_c^2)^{1/2}$$

for the family of parabolic cylinders.

The crossed-tangent method can also be applied to the parabolic cylinder. For the case of the paraboloid two orthogonal[1] tangents, $\bar{\rho}_\sigma$ and $\bar{\rho}_\zeta$, were used. Here, two orthogonal tangents, $\bar{\rho}_x$ and $\bar{\rho}_y$, serve the same purpose.

$$\bar{\rho} = \hat{i}\, x + \hat{j}\, y + \hat{k} \left(\frac{x^2}{4 F_c} + z_1\right), \quad (z_1 = \text{constant})$$

Then

$$\bar{\rho}_x = \hat{i} + \frac{x}{2 F_c} \hat{k}$$

and

$$\bar{\rho}_y = \hat{j},$$

which are obviously orthogonal, give the same $\bar{n}$ for the parabolic cylinder via

$$\frac{\bar{\rho}_x \times \bar{\rho}_y}{|\bar{\rho}_x \times \bar{\rho}_y|}.$$

Attention is called to the fact that normals to surfaces are sought for the vector Kirchhoff formulation. The selection of simple curves (Jordan arcs) lying in a given surface allows the computation of a disc of normals at each point on a

[1] The tangents for the paraboloid are obtained from an orthogonal net (σ, ζ). Verification of their orthogonality is seen in the vanishing dot product.

$$\bar{\rho}_\sigma \cdot \bar{\rho}_\zeta = \hat{i} \sin \zeta - \hat{j} \cos \zeta + \hat{k} \frac{\sigma}{2F} \cdot (\hat{i}\, \sigma \cos \zeta + \hat{j}\, \sigma \sin \zeta) \equiv 0.$$

curve. It is usually not obvious which of this infinity of normals at a point on the curve is also the unique normal to the associated surface. The risk of making an error here is obvious since at least two distinct curves are required through a common point before a surface normal can be defined. The intersection of two discs of normals is the desired surface normal. For the preceding reasons, single arcs will not be used here to infer surface normals.

The surfaces considered here are all simple and have unique normals with but one exception. A pair of normals exists at every point where panels are contiguous, corresponding to the normals of the "parent" parabolic cylinders. Practically, this causes no difficulty with the Kirchhoff integration in the program since normals are always taken in the interior of curvilinear quadrilaterals (differential areas). Implicitly, however, this represents a departure from rigor since the Green's theorem underlying the Kirchhoff formulation assumes continuous functions. In view of other approximations such as quantization of the illumination distribution, and the use of limited data on the surface, the departure is not considered serious. It is noted that a finite or mathematically open surface also represents a discontinuity. The Kottler contour integral which compensates for this is not considered here as the transverse far-fields are not affected.

NUMERICAL APPROACH TO SURFACE NORMALS

A somewhat more realistic simulation of the ATS-F deployable antenna is obtained by admitting distortion of the parabolic[1] ribs supporting the (metallized) reflecting mesh. If it is assumed that the reflecting mesh is defined by straight lines ($\bar{L}$) between supporting ribs[2], as shown in Figure 2, there are several ways of obtaining surface normals. All of the methods considered at this writing are predicated on the formation of a polynomial $z = P(y)$ for each supporting rib. It is anticipated that the number of data points describing a rib condition will be much smaller than the number of samples required in the radial direction to accomplish the integration of the Kirchhoff formulation. The discussion is restricted to a single panel throughout since the treatment for each panel is identical and the indexing of panels, to obtain the proper resolutes of the surface normals in 3-space, follows from simple rigid-body rotations of classical mechanics.[3] A Cartesian (x, y) net replaces the cylindrical (σ, ζ) net used with axially symmetric surfaces.

[1] Appendix A. It is shown that the intersection of a plane and a parabolic cylinder (F_c) is a parabolic arc (F_R) or rib. $F_R = F_c / \cos^2 \alpha$, where α is the panel half-angle.

[2] The straight-line assumption will be removed in the subsequent development.

[3] Ref. 4, page 107

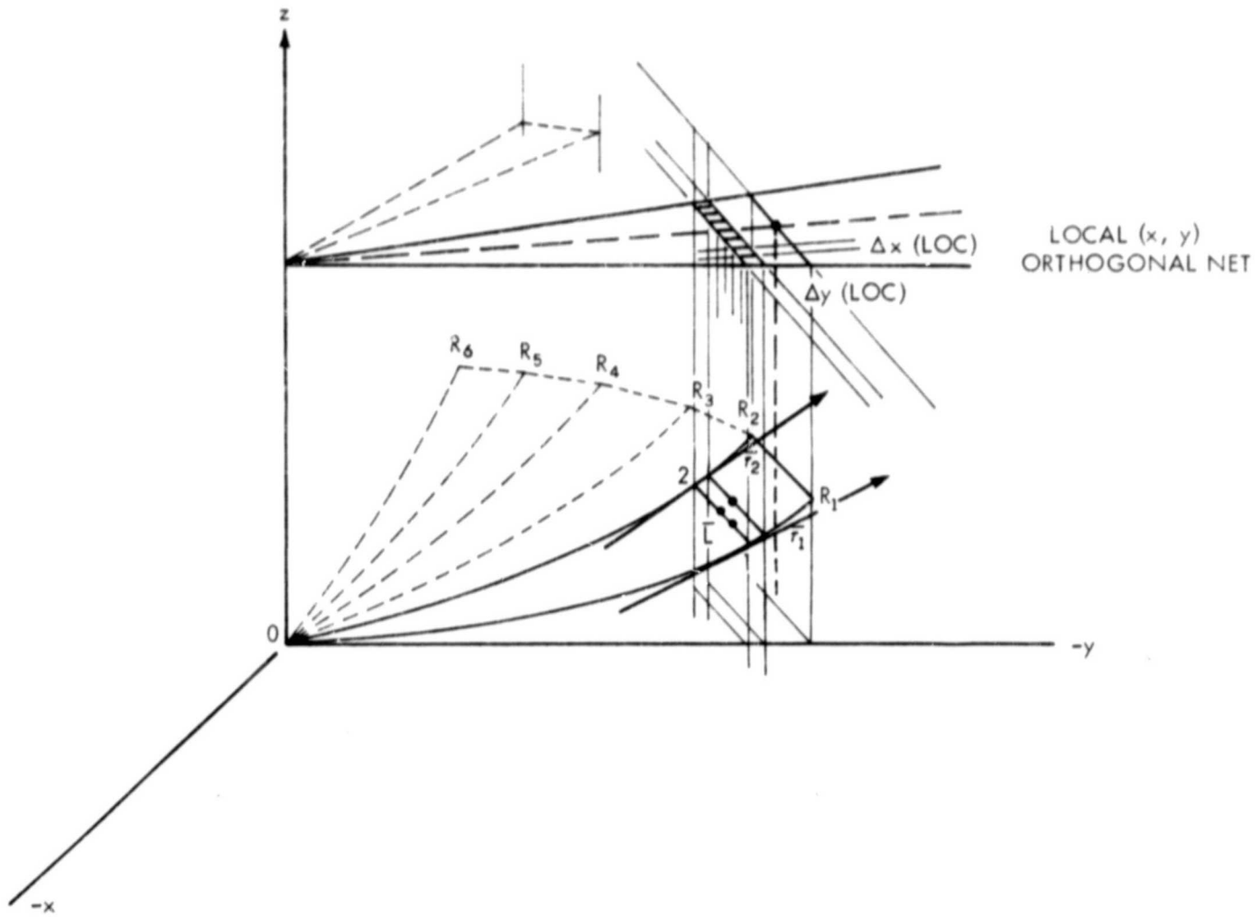

Figure 1. Paneled reflector with distorted ribs subdivided by means of a system of (x, y) coordinate nets

When rib coordinate data is given in Cartesian (x, y, z) form, a vector with origin at O represents a point on the rib and, therefore, on the panel. Rib data can be transformed[1] to the (-y, z) half-plane via the indirect transformation (A^{-1}) so that z = P(y), a polynomial in y alone, can be formed. This is effectively a rotation of the rib about the z-axis. If this operation is performed for all the ribs a number of elementary techniques[2], such as the direct-transformation (A), can be used in conjunction with the (x, y) net to provide rib coordinates (x, y, z) to as fine a resolution, or sampling, as may be required by the Kirchhoff method at a given frequency. Once the rib coordinate data (between given data points) is available, it is possible to write the components of the taut-mesh line $\bar{L}$ as the difference of rib position vectors $\bar{V}_1$ and $\bar{V}_2$. See Figure 1. This line is one of

[1] Ref. 4, pp. 108-109 describes the transformations A and A^{-1}.

[2] The details of the process are contained in the program listing.

the tangents to the distorted surface under the straight-line fabric assumption, and immediately suggests the first method for finding surface normals via an interpolation process.

An obvious means of obtaining a normal to the surface at a panel edge is to obtain another tangent somewhere, and use the method of crossed tangents, properly normalized. The polynomial P_1 (y) for rib R_1 can be differentiated to obtain the slope, $\bar{\tau}_1$, everywhere along that rib. Similarly, P_2 (y) for rib R_2 will supply another tangent, $\bar{\tau}_2$, but the latter vector must undergo a rotation transformation about the z-axis in the amount 2α, the panel angle. Tangents to the polynomials necessarily have a zero component in the x-direction since P_1 (y) is a function of y alone. It can be seen that the rib tangents are not, in general, orthogonal to the taut-mesh line $\bar{L}$. This does not preclude their application in the crossed-tangent technique for finding the normals to the surface. It is sufficient that two distinct tangents lying in a tangent plane have been found, and these uniquely determine the normal $\bar{n}$ at a point on the surface. With a normal $\bar{n}_1$ and $\bar{n}_2$ at either end of a strip of fabric, as shown in Figure 1, other intermediate normals are found by simple linear interpolation of the difference of the components of $\bar{n}_1$ and $\bar{n}_2$ along $L = |\bar{L}|$. As a special example, the difference

$$(n_{x1} - n_{x2})\,\hat{i} + (n_{y1} - n_{y2})\,\hat{j} + (n_{z1} - n_{z2})\,\hat{k} = (0,\ 0,0)$$

for the case of the parabolic cylinder panel so that no incremental correction to the normal at $\bar{n}_1$ is applied while traversing a strip of length L. The normal is everywhere the same between points 1 and 2, as it should be, for the indexed, ideal parabolic cylinder.

A second method of obtaining the normals to the distorted surface can easily be evolved from the preceding. The taut-fabric concept that regards the curve between points 1 and 2 as a perfectly straight line, mathematically, can now be removed. Since two tangents suffice to form the normal, three closely-spaced points lying on the surface of interest lead to a normal. If the surface is adequately specified and subdivided, by an (x, y) net here, three of the four coordinate triplets defining an increment, of area can be used to form a pair of difference vectors (i.e., tangents). Interpolation of the normals is not necessary by this method. The surface may be specified by a large amount of data on the rib and fabric positions or, alternatively, by a description of the curves between ribs (points 1 and 2). The latter may be empirically derived. Should the fabric happen to form straight lines as before, an interpolation, not of the normals to the surface, but one based on the z-coordinates at the end points of a strip can be

made. The 3-point, two-tangent approach for obtaining normals is obviously not restricted to an (x, y) net or panels, etc., but is generally applicable.

In conclusion, analytical methods are difficult to apply where surfaces are specified by data and auxilliary rules or equations. Methods which utilize the given data directly, or introduce the intermediate step of forming polynomials to obtain additional coordinates between data points, are therefore employed in the absence of an analytical surface description. A comparison of three distinct subroutines, representing varying degrees of departure from a parabolic cylinder, has been presented here:

(1) ideal parabolic-cylinder panel
(2) linear-mesh panel with distorted parabolic ribs
(3) arbitrary panel surface with distorted ribs.

An assumption throughout has been that the antenna has piece-wise (panel-wise) continuous derivatives.

INCREMENTAL AREA

The computation of incremental area for the paneled antenna is closely bound to the subject of surface normals. When analytical surface descriptions are available standard[1] methods apply. For example, the ideal parabolic cylinder panels can be treated by letting

$$x = u, \quad y = v, \quad z = \frac{u^2}{4 F_c}$$

so that

$$E = x_u^2 + y_u^2 + z_u^2 = 1 + \frac{x^2}{4 F_c^2}, \quad F = 0 \text{ (orthogonal net)}, \quad G = x_v^2 + y_v^2 + z_v^2 = 1$$

and[2]

$$d s = (E G - F^2)^{1/2} \, du \, dv = (y_2 - y_1) \left(1 + \frac{x^2}{4 F_c^2}\right) dx.$$

[1] Ref. 3, p. 13
[2] Ref. 1, p. 206

Then an incremental area can be evaluated as

$$\iint d\,s = s = (y_2 - y_1)\left[\frac{x}{4F_c}\sqrt{x^2 + 4F_c^2} + F_c \ln_e\left(\frac{x}{2F_c} + \frac{\sqrt{x^2 + 4F_c^2}}{2F_c}\right)\right]\Bigg|_{x_1}^{x_2}.$$

Several general expressions[1] can be written for ds, independent of any specific definition of surface. Using

$$\bar{n} = (\bar{\rho}_u \times \bar{\rho}_v)/(E\,G - F^2)^{1/2},$$

$$d\,s = (E\,G - F^2)^{1/2}\,du\,dv = |\bar{\rho}_u \times \bar{\rho}_v|\,du\,dv = \sec\angle(\bar{n}, \hat{k})\,du\,dv.$$

All three can be applied to the ideal parabolic cylinder, and lead to

$$\sec\angle(\bar{n}, \hat{k}) = \left(1 + \frac{x^2}{4F_c^2}\right)^{1/2}.$$

The last method is also applicable when distorted surfaces are encountered since the increment of area on the curved surface is related to the increment of area on the chosen planar net, the (x, y) net here, by a simple projection. Normals to the distorted surfaces are found by methods such as the non-orthogonal crossed-tangent approach, described previously. Then the angle between the base vector $\hat{k}$ and the normal to each increment of area can be computed and used to evaluate ds.

$$\underset{\text{(curved surface)}}{\Delta s} = \sec\angle(\bar{n}, \hat{k})\ \underset{\text{(planar-net area)}}{\Delta A}$$

[1] Ref. 1, pp. 208-209, Ref. 5 p. 48, Ref. 6, pp. 321-331, Ref. 7, pp. 81-83

The computation of ΔA is simple and depends on the net selected for the problem: (x, y), (σ, ζ), etc.

NUMERICAL INTEGRATION

The preceding sections dealt with the normals and the differential areas required by the Kirchhoff formulation, and these are now incorporated in the numerical integration. Since the original form for the backscattered field,

$$\bar{E}(x', y', z') = -\frac{j\omega\mu}{4\pi} \int_{S_1} \bar{n} \times \bar{H}_1 \psi \, ds$$

cannot be evaluated directly by purely analytical methods, in general, it is replaced by

$$\bar{E}(x', y', z') = -\frac{j\omega\mu}{4\pi} \sum_{\ell=1}^{m} \bar{n}_\ell \times \bar{H}_{1\ell} \psi_\ell \Delta S_\ell.$$

The continuous approach is, therefore, replaced by a discrete or quantized approach. For this reason no "master equation" is set down for the solution. The quantities $\bar{n}_\ell$, and ΔS_ℓ are properties of the specified surface: normals and curvilinear quadrilaterals of area. Illumination distribution $\bar{H}_{1\ell}$ and the phase-factor ψ_ℓ are determined by selecting the radiation source and the locus of pattern observation.

In the present ATS-F problem, a summation of the type shown above was performed for each of the 48 reflector panels. An (x, y) orthogonal net was convenient for subdividing the surface. There is no restriction on the method, however, and other geometries can be treated by the same process. Whenever possible, a coordinate net that is natural for the given geometry should be employed. Paraboloids for example, are most easily treated by a cylindrical or (σ, ζ) net, but this would be a poor choice for the ATS-F paneled reflector problem. Since the latter exhibits straight panel edges, an error in total area would be introduced by the (σ, ζ) net unless special devices were employed to delete certain (σ, ζ) quadrilaterals. At best, a residual error due to a saw-tooth edge would result.

The question of adequate sampling[1] of the surface arises since the continuous and discrete forms for $\bar{E}(x', y', z')$ are equal only in the limit as Δs_p becomes arbitrarily small. In the computer program an integration control constant designated LI (any positive real number) is made available to the program user. This number defines the maximum length of an edge of a curvilinear quadrilateral in wavelengths. For the present problem $\Delta x = \Delta y = LI\lambda$, and LI = 0.5 or 1.0 is usually adequate. The stability of solutions with respect to the sampling interval can be verified occasionally by computing a few field points at LI = 0.25, particularly for large observation angles (θ) from the reflector-system axis.

A program-related topic of great practical significance is the fitting of polynomials to given rib data. The least squares method was used to establish the coefficients of z = P(y) up to and including y^5. In order to verify the fit, an RMS figure is published by the program for each rib, and an overall RMS figure is provided for the set of ribs. For the present problem order 2 yielded the best fit for thermally distorted rib data at HOUR 11 and HOUR 4, the RMS value being less than .002 inch for the set of 48 ribs. The worst case observed yielded .007 inch RMS for one rib; the exact reason for the large RMS is unknown. Most individual ribs exhibited a polynomial fit well below the desired .005" criterion established by the ATS-F Project Manager for the 30-foot reflector.

PROGRAM INPUT-OUTPUT QUANTITIES

Program input can be separated into four groups as follows.

(1) Option Control Constants

These constants specify the number of feeds, the type of reflecting surface (paraboloid, paneled reflector, etc.), and the number of ribs, where applicable.

(2) Reflector Inputs

The parameters entered here are: maximum aperture radius, minimum aperture radius when a central region of the reflector is to be deleted, distance of the reflector "vertex" from the origin of coordinates, and focal length when a paraboloid or parabolic-cylinder paneled structure is selected. Data may be supplied in lieu of an analytical surface description.

[1] Ref. 8, pp. 321-323. The author discusses an antenna analogue to the classical sampling theorem of information theory by Shannon.

(3) Feed Inputs

For each of the specified feeds, the source strength, initial or starting phase, polarization vector components, directivity, and feed position/orientation are read in. The associated symbols are S_i, ψ_i , $\bar{e}_i$ or $\bar{h}_i$, N in $\cos^N\theta$, $\bar{\rho}_e$, and Euler angles α, β, γ. The operating frequency is also included here.

(4) Locus of Observation

Several choices can be made for the locus of observation of the radiation pattern. The usual one is a spherical locus given by range r = constant, angle ϕ = constant, and an angle θ = variable. Here $\theta_{min} \leq \theta \leq \theta_{max}$, and the increment $\Delta\theta$ determines the number of coordinate points at which the field is computed.

Program output can be separated into three groups as follows. A first page reiterates the input, thereby providing the program user a permanent record of the problem actually submitted to the computer. The second page, or group of pages, provides the Cartesian and spherical magnitudes and phases of the computed field quantities. The last page provides a summary of magnitudes of the Cartesian and spherical fields normalized about the maximum value which is set to zero decibels, arbitrarily.

COMPUTER REQUIREMENTS

The program is written entirely in FORTRAN for the IBM 360 Mod 91/95 systems at the Goddard Space Flight Center. It requires approximately 600 K bytes of core. The running time of a job depends on the type of problem, the number of field points, reflector size, sampling LI, operating frequency, and number of feeds.

For a typical problem with one field point, 30-foot reflector, LI = 1.0, frequency = 8.0 GHz, and a single feed, the computer time is approximately 30 seconds.

CRITICAL PROGRAM AREAS

This computer program has been correlated with well-known approximation functions, antenna slide rules, and measurements over a period of more than two years. Computed results agree favorably with those cases which allowed comparison in terms of beamwidth, side-lobe level, null position, and gain. Nevertheless, there are constraints which apply to the generation of radiation patterns

when using the program. Broadly stated, the Kirchhoff method fails when the size of the scattering object, its radius of curvature, and that of the wave, and the range of observation are small in terms of a wavelength. The failure is gradual. That is, when D, R_c, and r are 100 λ results are excellent. For 10 λ the solution is still useful, and at 1 λ the solution is probably valueless.

As indicated previously, the basis for the formulation assumes continuously varying functions. Increased departure from continuity will result in gradual degradation of the solution. The adequacy of the sampling interval should be verified occasionally with increasing θ. After the main beam and first sidelobe have been obtained the interval should be reduced to about half its original value.

COMPUTED RESULTS FOR ATS-F

A selected number of pattern cuts requested by the ATS-F Project will be presented here. The gain degradation of the paneled design-antenna, without the thermal distortion encountered in orbit, is given as a function of frequency in Figure 2. Degradation varies with frequency since a fixed physical departure of the paneled structure from a paraboloid becomes more significant (in terms of wavelengths) as frequency increases. A summary of gain degradation versus frequency is included with Figure 2. Input parameters and ancillary relationships are given below.

Input parameters to IBM 360/91:

focal length of parabolic cylinder F_c = 13.18180 ft.
feed position for paneled antenna F_m = +13.2 ft.
Sampling LI = 1.0
diameter of reflector D = 30.0 ft.
number of panels N' = 48.0
exponential N = 1.31250 in $\mathfrak{F} = \cos^N \theta$ (-10 db edge taper)
panel half-angle α = 3.75 degrees

Relationships used in computations

$F_R = F_c / \cos^2 \alpha$, where F_R equals rib focal-length

$F_m = F_R \dfrac{\sin 2\pi/N'}{2\pi/N'} = |z_1|$ for structure without unique focal-point.

Table 1

Paneled-Antenna Verification[1] on Axis ($\theta = 0°$)

Integration Net	Method[2]	Sampling (LI)	E_ϕ (db)
2 GHz			
(x,y) Cartesian	Parabolic Cylinder Panels	1.0	-81.487
(x,y) Cartesian	RFS	1.0	-81.475
(x,y) Cartesian	RFS	0.5	-81.486
(x,y) Cartesian	AFD	1.0	-81.475
(x,y) Cartesian	AFD	0.5	-81.486
(σ, ζ) Cylindrical[3]	Parabolic Cylinder Panels	1.0	-81.474
(σ, ζ) Cylindrical[3]	RM	1.0	-81.474
8.15 GHz			
(x,y) Cartesian	Parabolic Cylinder Panels	1.0	-81.704
(x,y) Cartesian	RFS	1.0	-81.701
(x,y) Cartesian	AFD	1.0	-81.701
(σ, ζ) Cylindrical[3]	Parabolic Cylinder Panels	1.0	-81.685
(σ, ζ) Cylindrical[3]	RM	1.0	-81.685

[1] Ideal Paraboloid reference Level = -81.463 db.

[2] The AFD method utilizes tangents at opposite sides of a panel and a fabric line to obtain the normal, while the RFS method is the 3-point, 2-tangent approach. The RM method is similar to the AFD method in that normals are obtained by an interpolation process.

[3] (σ, ζ) option leads to excess areas beyond panels

The preceding results were obtained by several of the analytical/numerical techniques described previously. Table 1, above, indicates the results of some of the comparisons.

Distortion of the 30-ft reflector in orbit as a function of the reflector attitude with respect to the sun has been computed by others for each position in the 24 hour period orbit. Two representative cases are hours 11 and 4. Illumination edge tapers were set at -10 db, and linear polarization was used in all the following computations.

The behavior of the paneled antenna under thermal load at Hour 11 and Hour 4 is now given at 2.0 GHz and 8.15 GHz. At each frequency a pattern cut

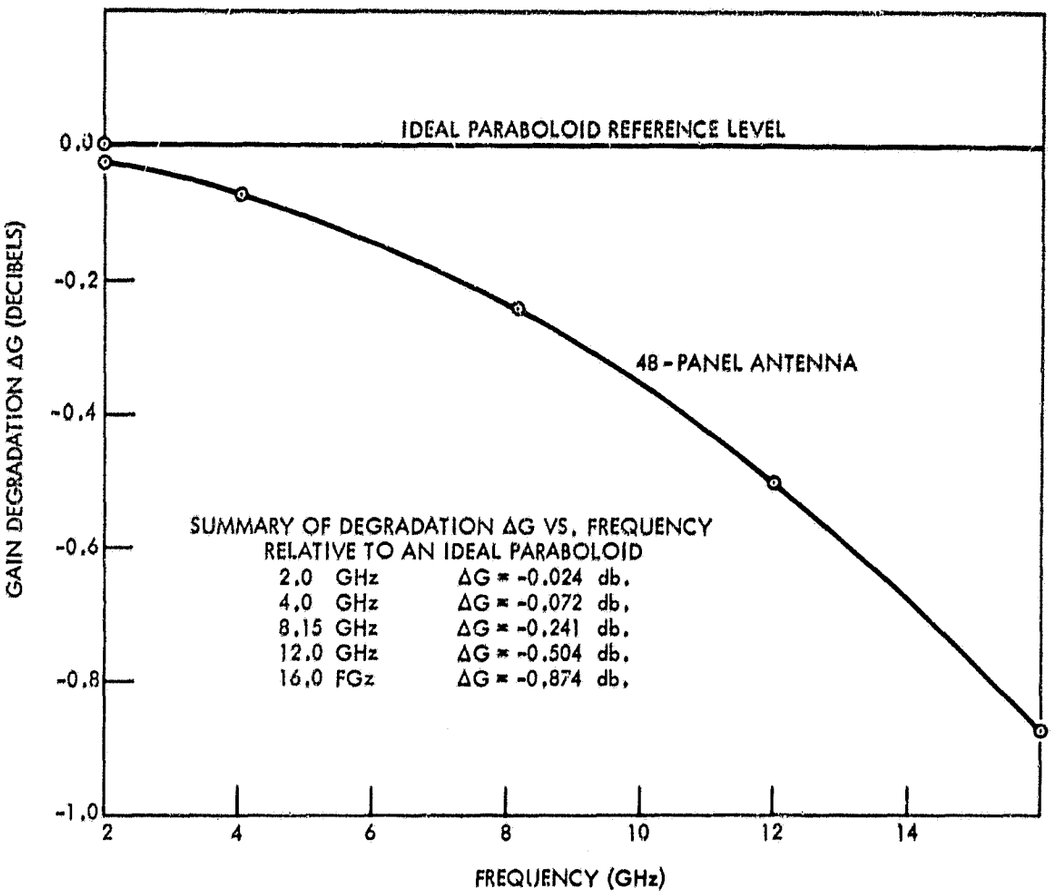

Figure 2. Gain degradation Δ G vs frequency for 30-ft ATS-F antenna

on an ideal focal-point paraboloid and an undistorted, optimally-fed paneled antenna are provided to serve as a basis for comparison. Figures 3 and 4 are the paraboloid and paneled-reflector reference patterns at 2.0 GHz, while Figures 5 and 6 show results at Hour 11 and Hour 4, respectively, for that frequency. It can be seen that the paneled antenna is a very good approximation to a paraboloid at 2.0 GHz. The principal differences in computed results are a slight perturbation of the phase plot and increased level of the cross-polarized energy due to the panel effect. Cross-polarized levels for the ideal paraboloid were extremely low and are not plotted.

At Hour 11 and Hour 4 the reflector performance at 2 GHz is seen to be affected only slightly. A part of a planar cut along the line of symmetry for the thermal distortion is given in Figures 5 and 6 to illustrate beam widening (4%) and axial shift due to reflector distortion. Further effects on phase characteristics and cross-polarization levels are in evidence but these are realtively minor perturbations of the beam characteristics.

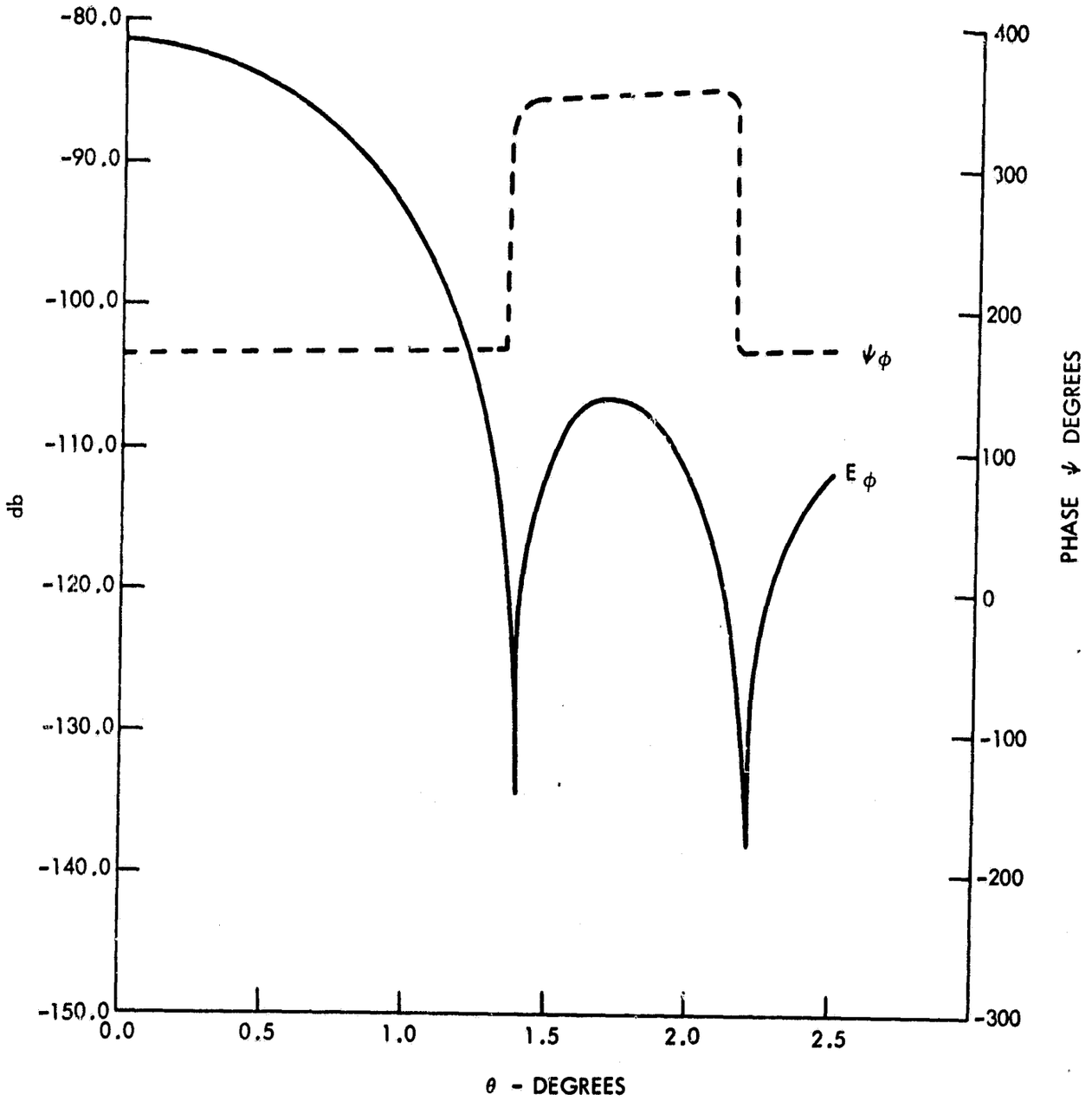

Figure 3. Focal-point fed ideal parboloid (2.0 GHz)

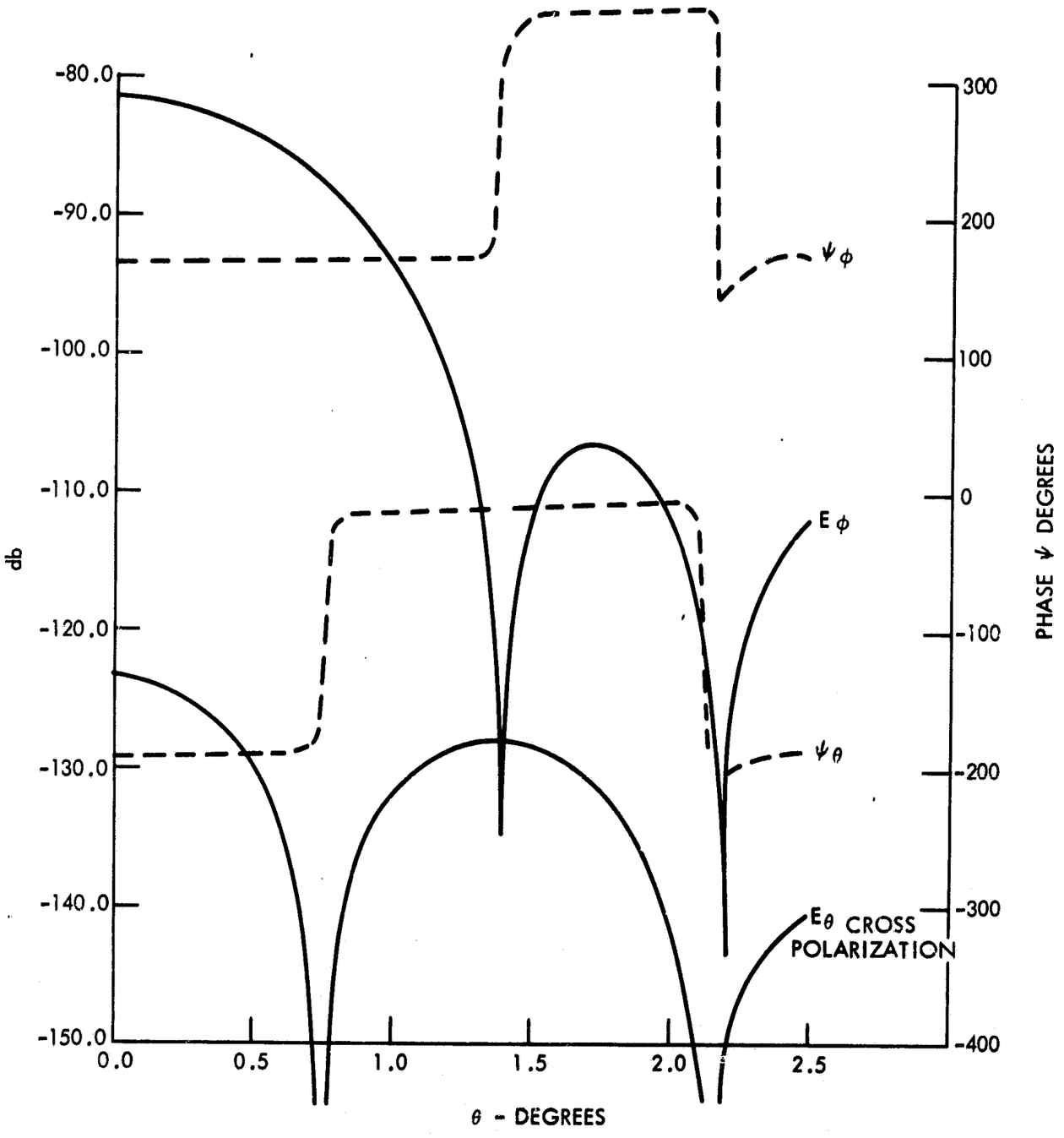

Figure 4. Optimally-fed paneled antenna (2.0 GHz)

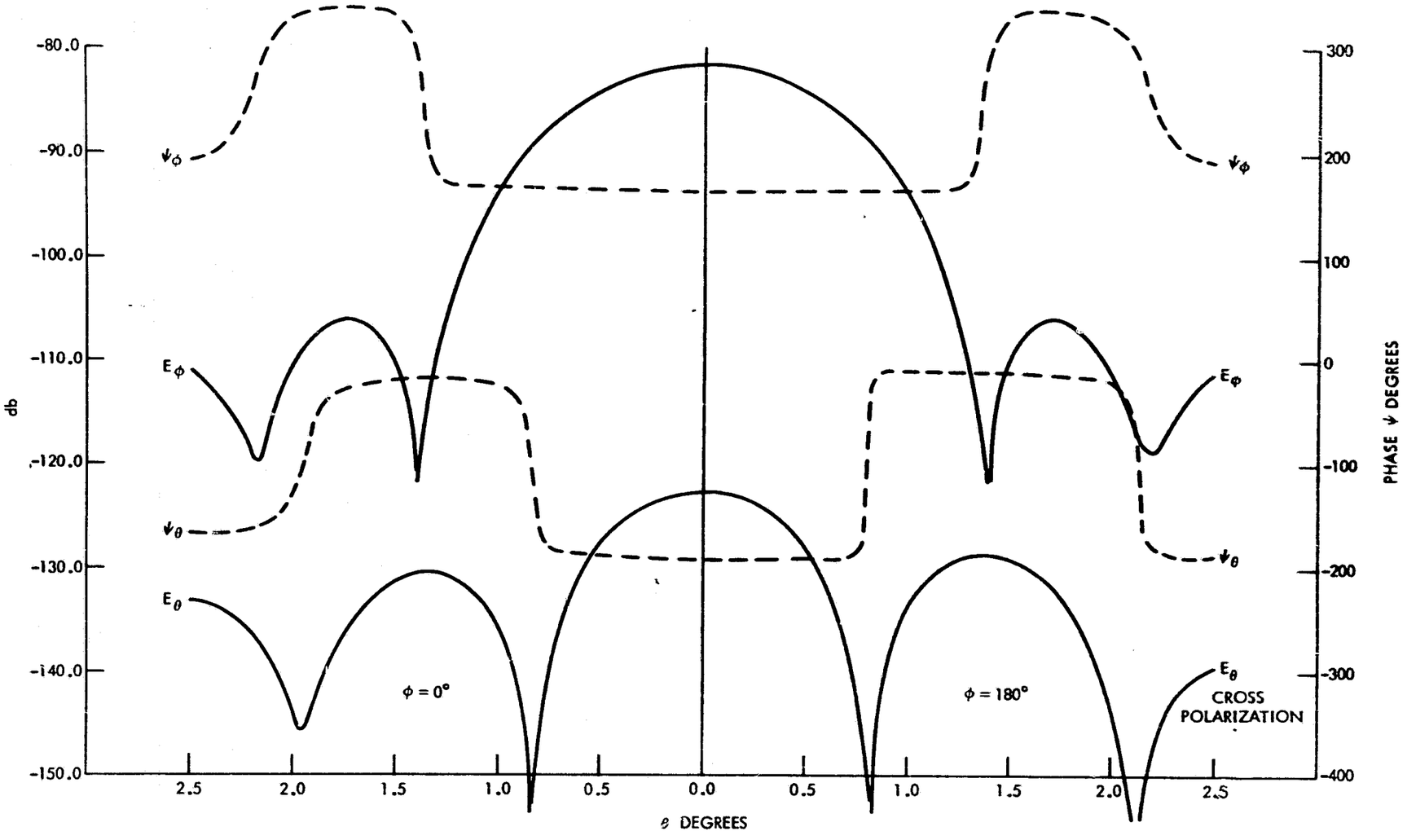

Figure 5. Paneled-antenna with HOUR-11 distortion (2.0 GHz)

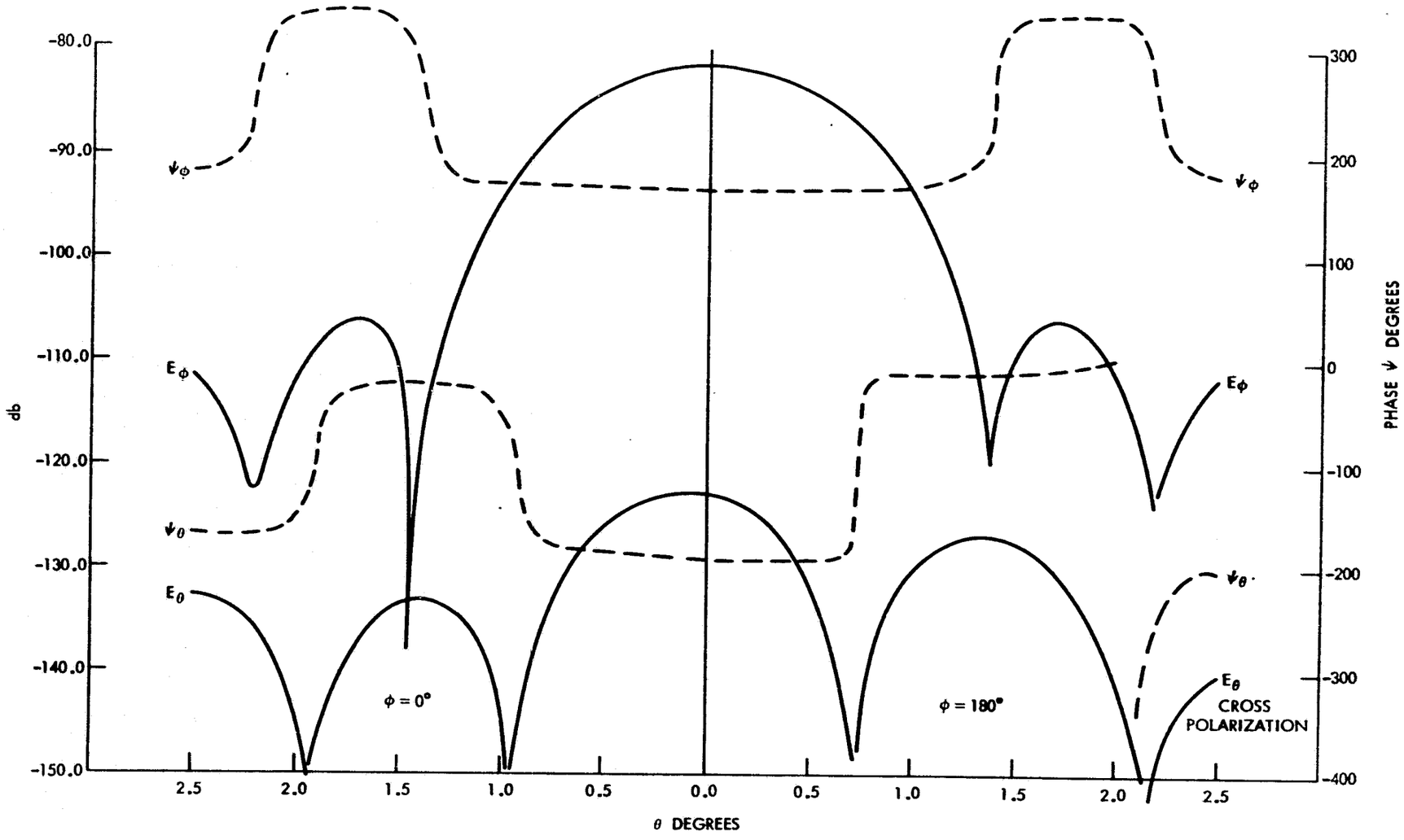

Figure 6. Paneled antenna with HOUR-4 distortion (2.0 GHz)

Proceeding to the higher frequency, 8.15 GHz, Figures 7 and 8 are the paraboloid and paneled-reflector reference patterns while Figures 9 and 10 show results at Hour 11 and Hour 4, respectively, at this frequency. The paneled antenna is still a very good approximation to a paraboloid at 8.15 GHz. For the pattern cut shown, negligible beam broadening appears. The phase characteristic is now highly asymmetric, as is the cross-polarization pattern. Since the ideal paraboloid cross-polarization levels at 8.15 GHz were reported as about -80 db relative to the principal polarization $E_{\theta_{max}}$ these were not plotted. Null-filling is seen to be more severe at 8.15 GHz than at 2.0 GHz.

Table 2, below, indicates the results of some comparisons made among the different analytical/numerical techniques for the thermally distorted surfaces at Hour 11 and Hour 4.

Table 2

Thermally-Distorted Paneled-Antenna Verification on Axis ($\theta = 0°$)

Integration Net	Method	Sampling (LI)	E_ϕ (db)	$\Delta G = G_{paneled} - G_{distorted-paneled}$ (db)
2 GHz, Hour 11				
(x,y) Cartesian	RFS	0.5	-81.495	0.009
(x,y) Cartesian	AFD	0.5	-81.498	0.013
(x,y) Cartesian	AFD	0.25	-81.502	0.017
(σ, ζ) Cylindrical	RM	0.5	-81.490	0.016
8.15 GHz, Hour 11				
(x,y) Cartesian	RFS	1.0	-81.903	0.202
(x,y) Cartesian	AFD	1.0	-81.908	0.207
(x,y) Cartesian	AFD	0.5	-81.913	0.212
(σ, ζ) Cylindrical	RM	1.0	-81.896	0.211
2 GHz, Hour 4				
(x,y) Cartesian	RFS	0.5	-81.496	0.010
(x,y) Cartesian	AFD	0.5	-81.501	0.015
8.15 GHz, Hour 4				
(x,y) Cartesian	RFS	1.0	-81.931	0.230
(x,y) Cartesian	AFD	1.0	-81.939	0.238

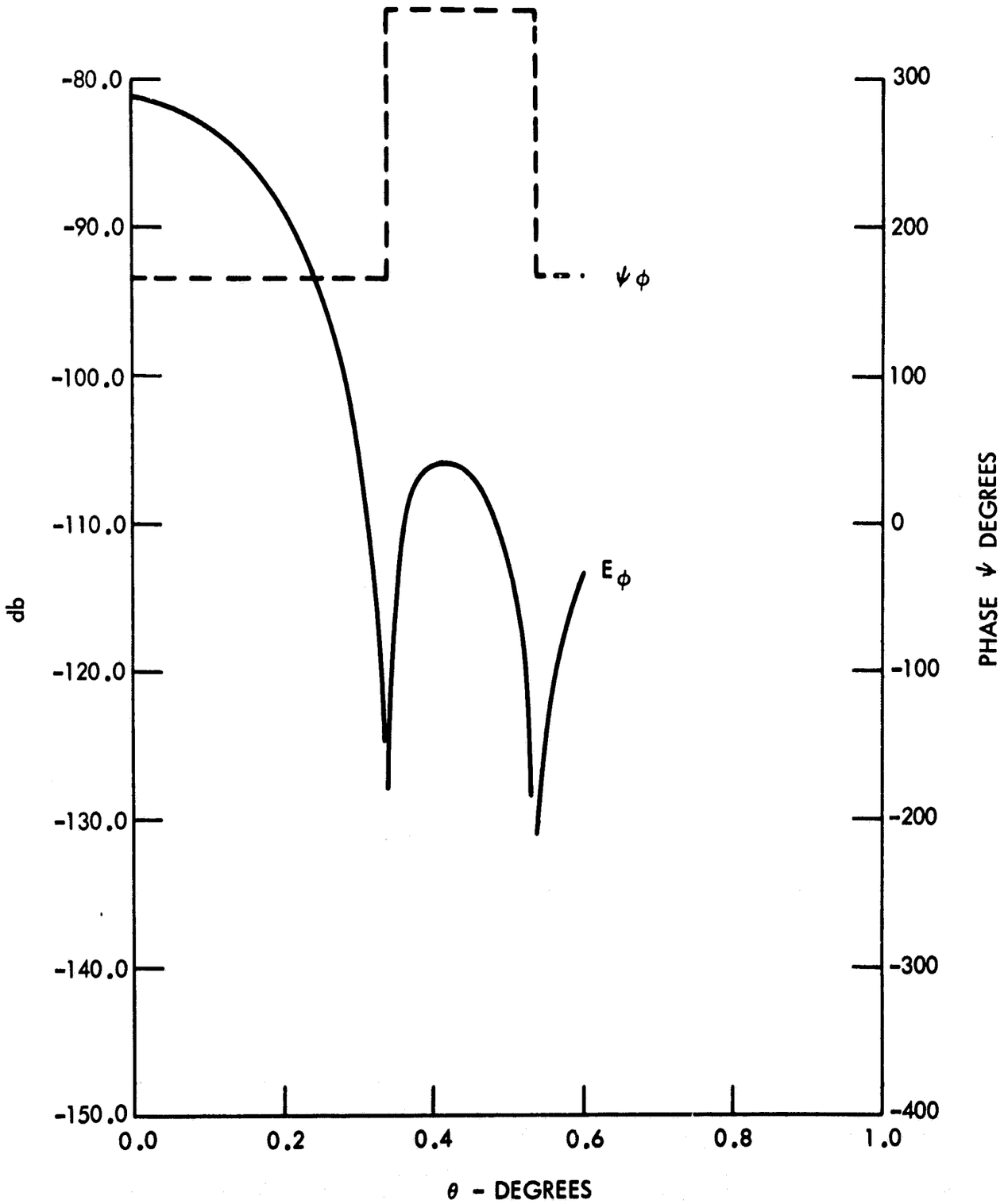

Figure 7. Focal-point-fed ideal paraboloid (8.15 GHz)

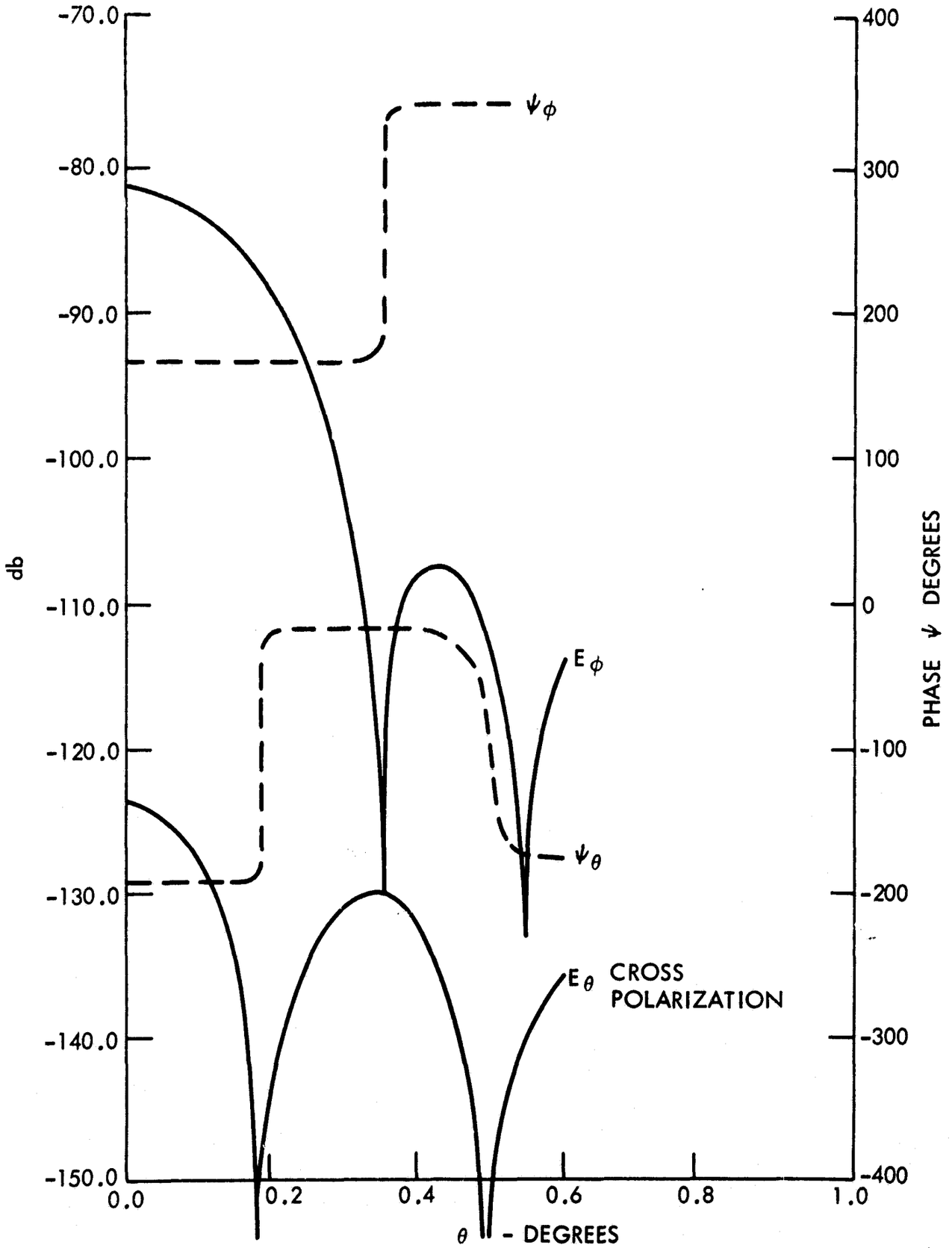

Figure 8. Optimally-fed paneled antenna (8.15 GHz)

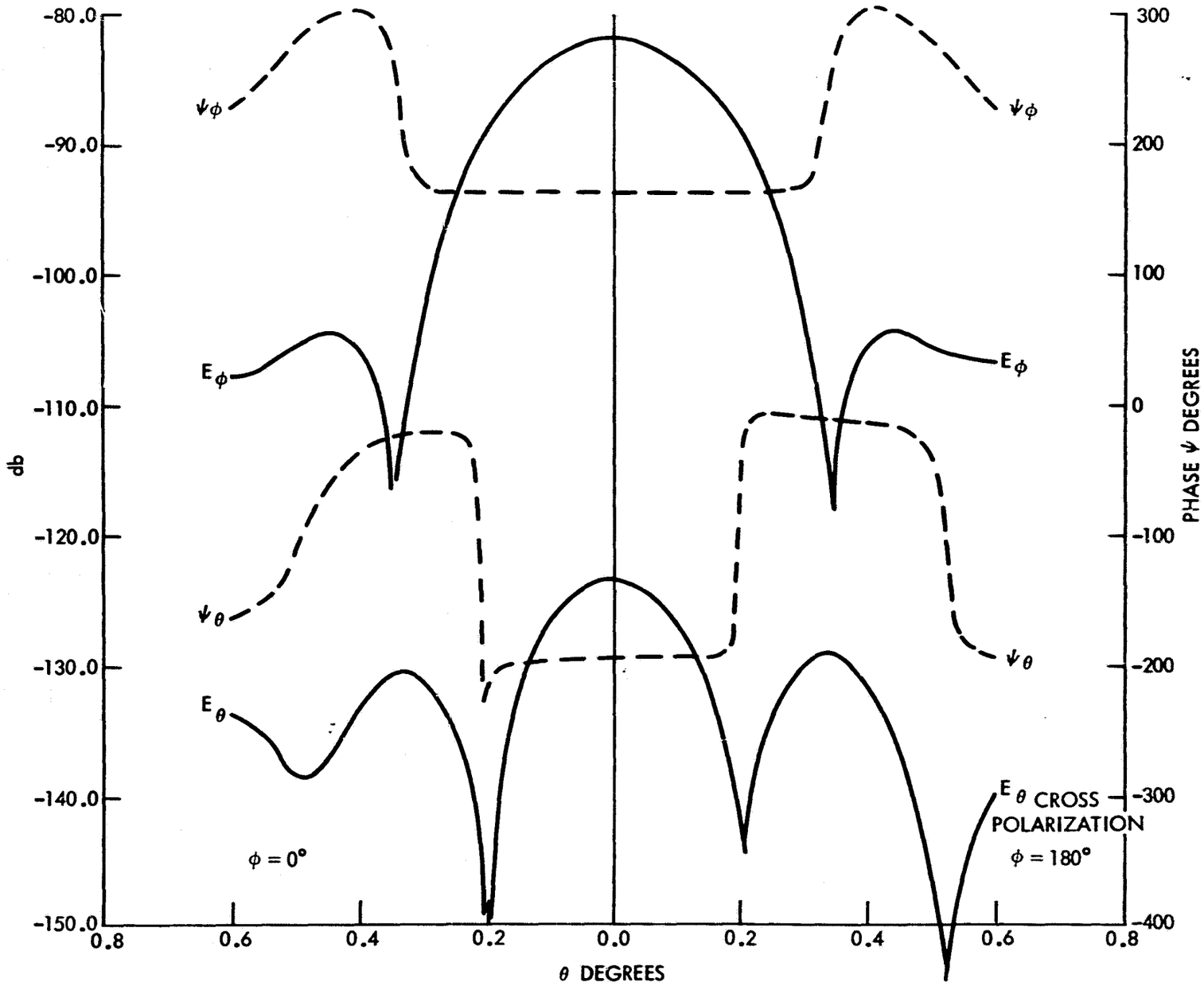

Figure 9. Paneled antenna with HOUR-11 distortion (8.15 GHz)

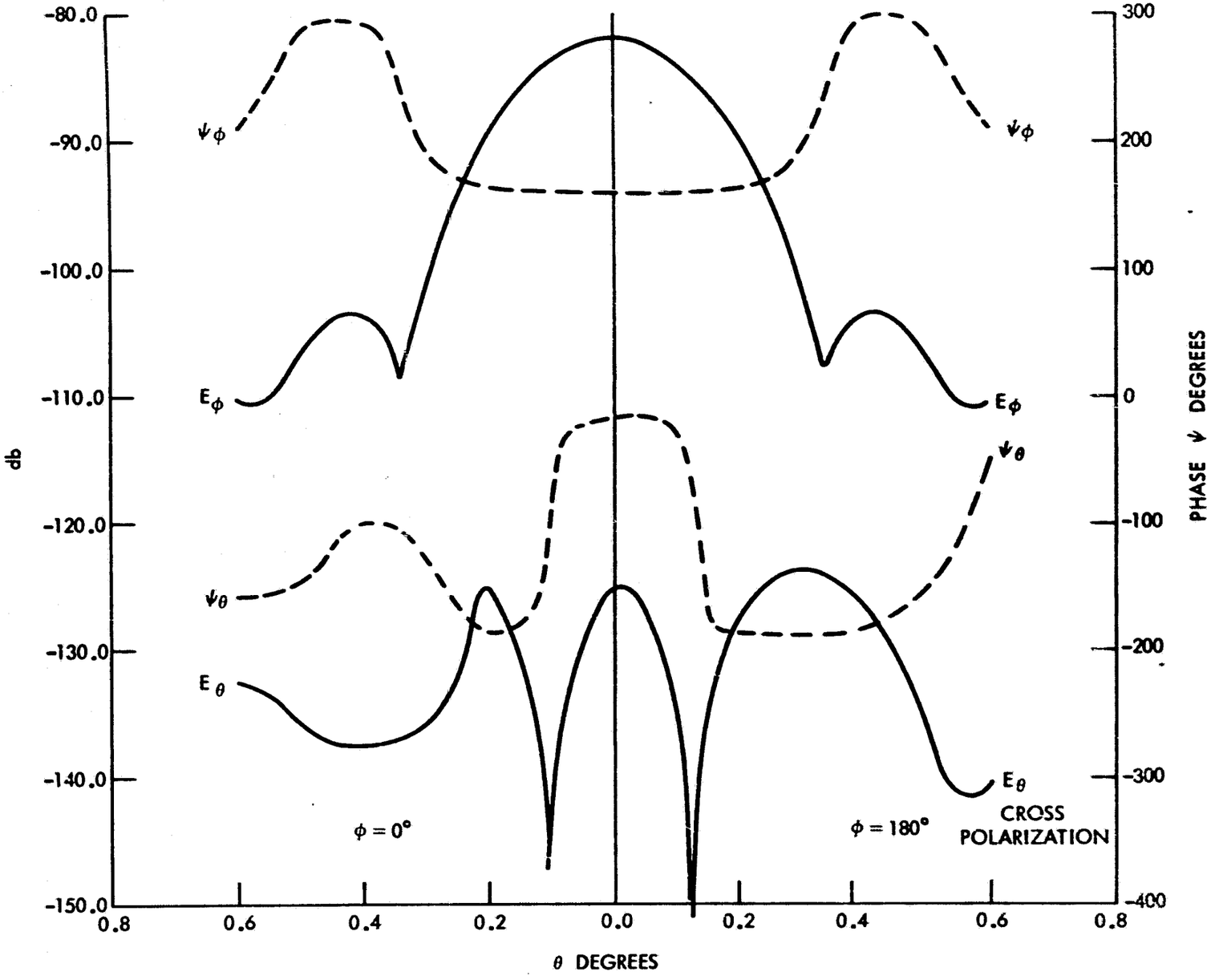

Figure 10. Paneled antenna with HOUR-4 distortion (8.15 GHz)

Additional detailed comparisons were made, for the normals to the surfaces by different methods for example, but these are not presented here. Comparison of the general methods, for the special case of zero distortion, with the elementary parabolic cylinder panel approach has served to establish the validity of the general methods.

SUMMARY

This document describes the analytical and numerical methods that were employed in obtaining the far-field or Fraunhofer radiation patterns for the ATS-F paneled reflector antenna via vector Kirchhoff theory. The emphasis throughout has been on using analytical methods whenever practicable, and numerical methods for the description of distorted surfaces and subsequent integration. A gradual transition was made from paraboloid to a paneled antenna, composed of portions of a parabolic cylinder, and finally to a distorted paneled antenna. By this means the analysis is justified, and numerical verification can be obtained at various levels of the development. For example, the components of the normals, the increments of area, and finally the computed field values can be compared in the transition.

Although this task was undertaken to obtain solutions for a specific ATS-F geometry (D = 30 ft., N = 48 panels, f = 2.0, 8.15 GHz, etc.) the program is general in nature and can accept parameter changes without any modification. The assumption of straight fabric lines is not essential, and the methods for dealing with doubly curved surfaces are available. At this time, the more general option has not been implemented since it is not known whether adequate coordinate data or empirical curves between supporting ribs will be used to describe the surface to the resolution required by the sampling theorem. Feed geometry can also be changed to include monopulse configurations, line feeds, etc. without any modification of the basic program.

ACKNOWLEDGMENTS

The authors acknowledge the assistance received through discussions with Mr. Harry Gerwin, ATS-F Project Manager, and other members of the Project team. In addition, helpful comments were received from members of the Antenna Systems Branch, ADD. Finally, the authors would like to acknowledge the contribution of Mrs. Rose Kirkpatrick of C.A. Inc. who provided the computed radiation patterns using the IBM 360/91 system at Goddard Space Flight Center.

REFERENCES

1. Kaplan, W., "Advanced Calculus," Addison-Wesley Publishing Company, Inc., 1959.

2. Javid, M. and Brown, P. M., "Field Analysis and Electromagnetics," McGraw-Hill Book Company, Inc., 1963.

3. Schmidt, R. F., "The Calculation of Antenna Radiation Patterns by a Vector Theory Using Digital Computers," GSFC (X-525-68-315), August 1968.

4. Goldstein, H., "Classical Mechanics," Addison-Wesley Publishing Company, Inc., 1959.

5. Wilson, E. B., "Vector Analysis (Gibbs)," Yale University Press, 1929.

6. Kreyszig, E., "Advanced Engineering Mathematics," John Wiley and Sons, Inc., 1962.

7. Coburn, N., "Vector and Tensor Analysis," The MacMillan Company, 1955.

8. Skolnik, M. I., "Introduction to Radar Systems," McGraw-Hill Book Company, Inc., 1962.

APPENDIX A

THE INTERSECTION OF A PARABOLIC CYLINDER AND A PLANE

Parametric equations for a paraboloid (F):

$$x = \sigma \sin \zeta,\ y = -\sigma \cos \zeta,\ z = \frac{\sigma^2}{4F} + z_1$$

Parametric equations for a parabolic cylinder (F_c): when

$\zeta = 90°,\ z_1 = 0$:

$x = \sigma,\ y =$ any value, $z = \frac{\sigma^2}{4F_c}$

$\therefore z = \frac{x^2}{4F_c}$ for a parabolic cylinder (for all values of y).

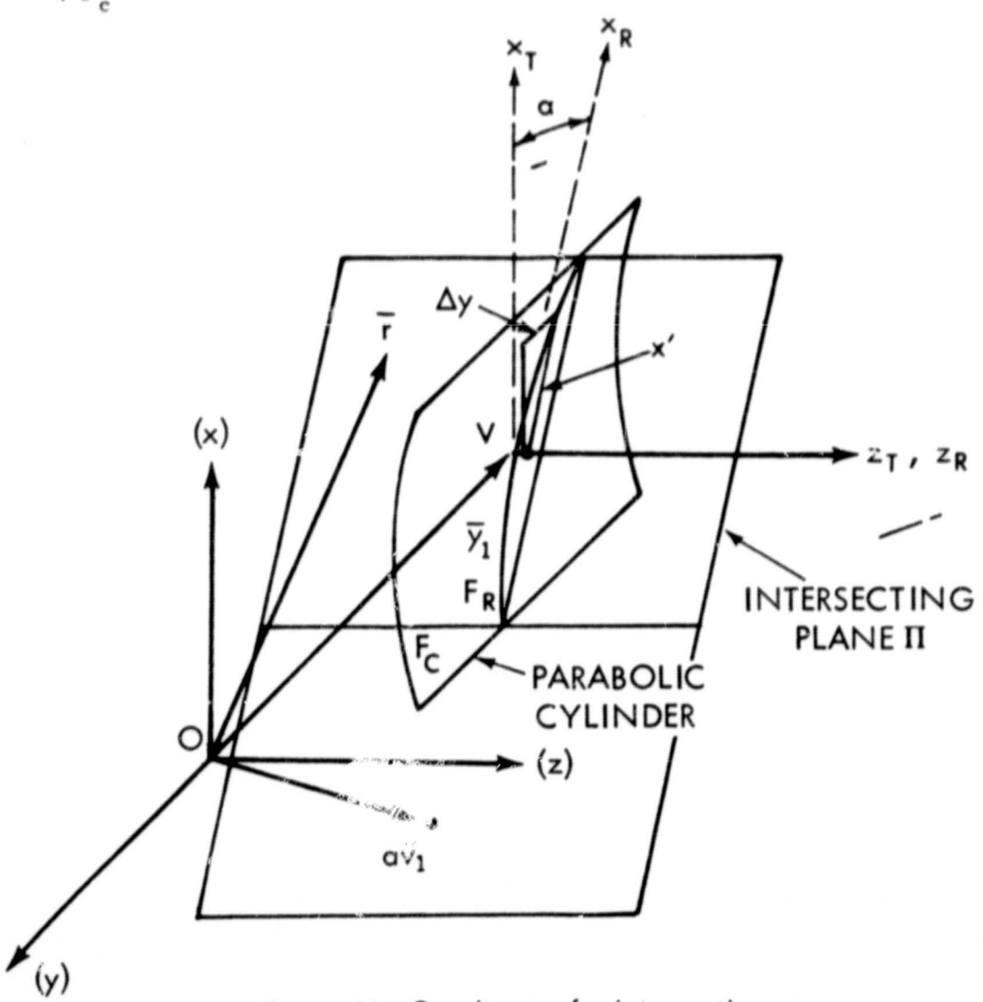

Figure 11. Coordinates for intersection

equation of the intersecting plane (Π):

$$\bar{r} \cdot \bar{v}_1 = a = x\, v_x + y\, v_y + z\, v_z$$

$\bar{r}$ = generic vector on Π

$\bar{v}_1$ = unit vector orthogonal to $\Pi = v_x\, \hat{i} + v_y\, \hat{j} + v_z\, \hat{k}$ and $(v_x^2 + v_y^2 + v_z^2)^{1/2} = 1$

a = minimum distance to Π, a scalar

A simultaneous solution of the equations for parabolic cylinder and plane yields the equation of their intersection. If $v_z = 0$, then Π contains the displaced z-axis through vertex point V as shown above. The intersection assumed here is then not of the most general type. Substituting x from the equation for the plane into the equation for the parabolic cylinder gives:

$$z = \frac{1}{4\, F_c}\left[\frac{a - y\, v_y - z\, v_z}{v_x}\right]^2 \quad \text{for the intersection } (\cap).$$

The singularity at $v_x = 0$ poses no problem since it represents the trivial case of the intersection between the two surfaces.

Now the displacement of V from O is

$$\bar{\rho}_\epsilon = \hat{i}\, x_1 + \hat{j}\, y_1 + \hat{k}\, z_1 = \hat{j}\, y_1 = \bar{y}_1,$$

above, and

$$\bar{\rho}_\epsilon \cdot \bar{v}_1 = x_1\, v_x + y_1\, v_y + z_1\, v_z = y_1\, v_y = a.$$

The arbitrary separation $\bar{y}_1$ between O and V can be eliminated by letting $y = y_1 + \Delta y$ so that

$$z = \frac{1}{4F_c}\left[\frac{y_1 v_y - (y_1 + \Delta y) v_y - z v_z}{v_x}\right]^2 = \frac{1}{4F_c}\left[-\frac{\Delta y\, v_y}{v_x}\right]^2 \quad \text{for } \cap.$$

But $\tan \alpha = v_x/v_y$, where α is the angle Π makes with the displaced xz-plane. Also, $\Delta y = x' \sin \alpha$ where x' is the distance from a point on $\cap$ to the displaced z-axis. Then $z = x'^2/4(F_c/\cos^2 \alpha)$ for the intersection, which represents a parabolic arc lying in plane Π. The focal-length of this parabolic arc is $F_R = F_c/\cos^2 \alpha$. For a reflector composed of indexed portions of a parabolic cylinder F_c, α becomes the panel half-angle.

APPENDIX B

ILLUMINATION EDGE-TAPER FOR FOCAL-POINT-FED PARABOLOIDS

The parametric-equations for a paraboloid with vector at $z_1 = -F$ are

$$x = \sigma \sin \zeta,\ y = -\sigma \cos \zeta,\ z = \frac{\sigma^2}{4F} + z_1 = \frac{\sigma^2}{4F} - F$$

Since γ_i is symmetric about z, take $\zeta = \pi/2$ without loss of generality. The field at vertex V is $E_1 \propto \mathcal{F}(\Theta)/F$. The field at some edge (σ) is

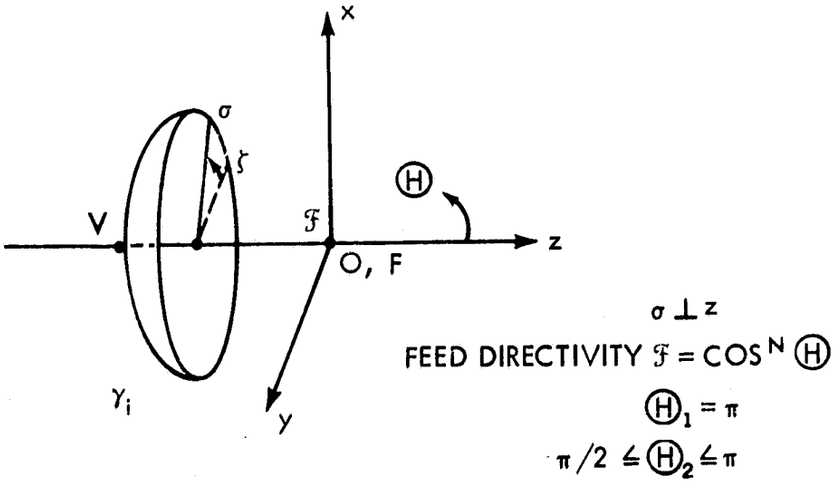

Figure 12. Cylindnical Coordinates

$$E_2 \propto \frac{\Im \Theta_2}{(x^2 + z^2)^{1/2}} = \frac{4F \Im \Theta_2}{\sigma^2 + 4F^2}.$$

Then,

$$db = 20 \log_{10} \frac{E_1}{E_2} = 20 \log_{10} \left(\frac{\sigma^2 + 4F^2}{4F^2} \right) + 20N \log_{10} \frac{\cos \Theta_1}{\cos \Theta_2}$$

(space taper) (feed taper)

or

$$db = 20 \log_{10} \left(\frac{\sigma^2}{4F^2} + 1 \right) + 20N \log_{10} \left(\frac{4F^2 + \sigma^2}{4F^2 - \sigma^2} \right)$$

(space taper) (feed taper)

In the above, $db \geq 0$, and the equation can be used to determine N for a specified edge taper or, conversely, to determine the edge taper if directivity is known.

APPENDIX C

POWER INTERCEPTED BY REFLECTOR USING $\mathfrak{F}(\Theta) = \cos^N \Theta$

Since $-\infty < N < +\infty$, the effect of N on the energy incident upon a reflector is of interest. For $0 < N < +\infty$, the maximum value of the feed function is always unity (bounded above) and occurs at $\Theta = 0$. Interest is restricted to the half-space $0 \leq \Theta \leq \pi/2$ in the present discussion[1] to avoid the generation of complex values for $\mathfrak{F}(\Theta)$. For $-\infty < N < 0$, the minimum value of the feed function is always unity (bounded below) and occurs at $\Theta = 0$. For $N = 0$, an isotrope (in amplitude) is obtained. See Figure 13.

The use of $\mathfrak{F}(\Theta) = \cos^N \Theta$ in a computer program therefore directs varying amounts of energy at the reflector, depending on the value of N chosen. For some studies this is undesirable, and a constant energy to the reflector is preferred. A simple integration over the appropriate solid-angle allows computation of coefficient(s) S, such that $\mathfrak{F}(\Theta) = \cos^N \Theta$ will direct equal energy at the antenna surface (single focal-point feed, here). In general, total energy $\mathfrak{E}_T$ is proportional to

$$\int_{\Theta=0}^{\Theta_2} \int_{\Phi=0}^{2\pi} S^2 \cos^{2N}\Theta \sin\Theta \, d\Theta \, d\Phi = -\frac{2\pi S^2}{2N+1} \cos^{2N+1}\Theta \Big|_0^{\Theta_2}$$

$$= \frac{2\pi S^2}{2N+1}(1 - \cos^{2N+1}\Theta_2), \quad 0 \leq \Theta_2 \leq \pi/2.$$

Suppose that S = 1 (reference) and N = m for a first case and N = n for a second case. Equating energies leads to

$$S = \left[\frac{2n+1}{2m+1} \; \frac{(1 - \cos^{2m+1}\Theta_2)}{(1 - \cos^{2n+1}\Theta_2)}\right]^{1/2},$$

the required coefficient for the second case.

[1] The FORTRAN program actually forms $\mathfrak{F}(\Theta) = |\cos\Theta|^N$, which effectively avoids complex values for $\mathfrak{F}(\Theta)$. If several feeds are employed, initial phase is introduced independently for the array via ψ_1 in $\Sigma S_i \cos^N i\Theta_i e^{-j\psi_i}$. The energy over a solid angle can still be obtained, but not as simply as above.

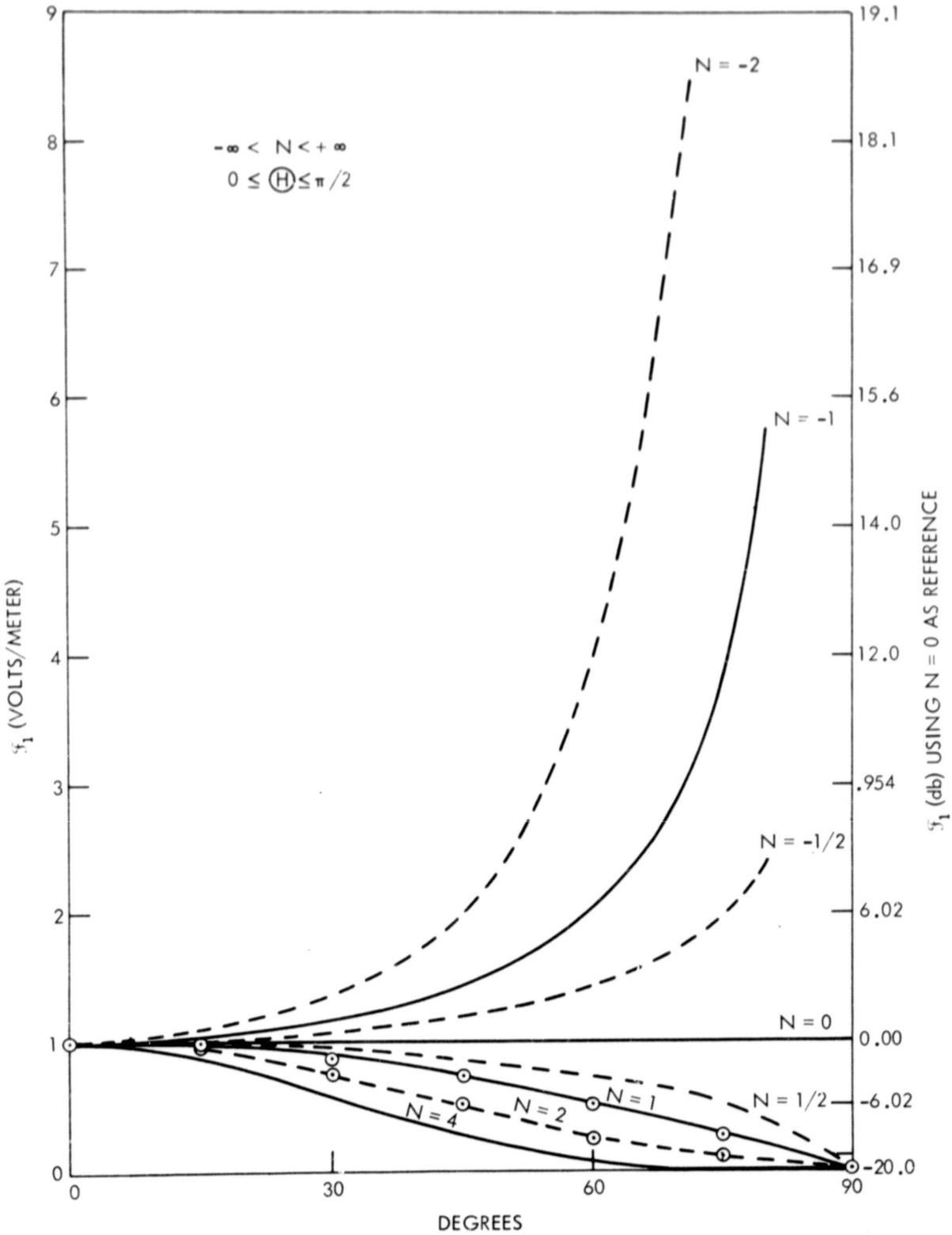

Figure 13. Prime-feed function $\mathfrak{F} = \cos^H \Theta$